Bulletin of the New Zealand Society for Earthquake Engineering, Vol. 57, No. 2, June 2024

A COMPARATIVE INVESTIGATION ON EXPERIMENTAL LATERAL BEHAVIOUR OF BARE RC FRAME, NON-STRENGTHENED AND FERROCEMENT STRENGTHENED MASONRY INFILLED RC FRAME

Debasish Sen[1], Fatema-Tuz-Zahura[2*], Anik Das[3], Hamood Alwashali[4], Md. Shafiul Islam[5], Masaki Maeda[6], Matsutaro Seki[7] and Muhammad Abdur Rahman Bhuiyan[8]

(Submitted *July 2023*; Reviewed *September 2023*; Accepted *December 2023*)

ABSTRACT

Although concrete framed structures are widely used with masonry infills, the contribution of masonry infills in structural design is limited to their dead loads only. Therefore, the full-fledged stiffness characteristics of masonry infill are not often considered. However, recent earthquakes showed the impact of masonry infill on the lateral behavior of surrounding RC frames. Moreover, sometimes existing masonry infills are strengthened using Ferrocement (FC), Textile Reinforced Mortar (TRM), Carbon Fiber Reinforced Polymer (CFRP), etc., which might also have a similar impact on surrounding RC frames. The impact includes enhanced shear demand, damage, etc. However, the effect of the enhanced shear demand on RC columns is a relatively less investigated issue. In this context, an experimental program was designed to compare the effect of non-strengthened and FC strengthened masonry infill on the behavior of the surrounding RC frame in terms of lateral strength, hinge formation, shear demand enhancement, and damage to columns. The test specimens, including a bare RC frame, a masonry infilled RC frame, and a FC strengthened masonry infilled RC frame, were subjected to a quasi-static cyclic lateral loads. The experimental result showed that the masonry infill and FC strengthened masonry infill increased lateral strength, on average, by 81% and 244%, respectively, when compared to that of the bare RC frame. Meanwhile, FC strengthening of masonry infill improved the lateral strength, on average, by 90% when compared with the masonry infilled RC frame's lateral strength. In this study, low-strength masonry infill caused the formation of a short column on the tension column of the RC frame. The application of ferrocement to low-strength masonry altered the position of the plastic hinge formed on the tension column of the RC frame when compared to that of the masonry infilled RC frame. Therefore, ferrocement strengthening of masonry eliminated the short column phenomenon in this particular study. Nevertheless, the shear demand (in terms of strain on the column tie) enhancement of the tension column was not substantial due to the ferrocement strengthening of the masonry infill when compared to that of the masonry infilled RC frame. Moreover, the damage concentration on RC columns (i.e., residual crack width) after insertion of masonry infill and ferrocement strengthened masonry infill changed to a smaller extent when compared to the bare RC frame damages, where the residual crack widths were within 1.0 ~ 2.0 mm.

https://doi.org/10.5459/bnzsee.1656

INTRODUCTION

Worldwide, seismically vulnerable building stock includes many masonry infilled RC framed buildings. Masonry infill is being utilized as a partition wall because of the availability of bricks locally. Although RC framed structures are widely used with masonry infill walls, the contribution of infill walls in structural design is limited to their dead loads only. Therefore, the full-fledged stiffness characteristics of masonry infill are not often considered. However, the previous experimental research [1-10] indicates the upgradation of the lateral capacity of RC frames by the insertion of masonry infill. In addition, several researchers [11-17] investigated additional shear demand on the surrounding RC column resulting from masonry infill under lateral loads. Moreover, past earthquakes demonstrated both beneficial and detrimental effects of masonry infill, which is reflected in post-earthquake studies [18-24]. Many masonry infilled RC frame buildings suffered damages due to the in-plane and out-of-plane collapse of masonry infills and the soft-storey failure mechanism [20, 25]. During in-plane damage, infill masonry walls exhibit three possible failure mechanisms, i.e., sliding shear failure along masonry layers, diagonal tension and compression strut failure, or sliding shear failure of adjacent RC columns [24]. In addition, corner crushing was also observed in previous seismic events [25]. For example, extensive cracking of infill walls was typically observed in the L'Aquila earthquake [22], whereas both sliding and corner crushing were observed in the Gorkha earthquake in Nepal [25]. However, such masonry infills contributed resisting seismic action up to damage occurrence by stiffening the framed structural system, while the story mechanism happened after the collapse of all the infill walls placed at the same floor level [22]. Furtado et al. [25] mentioned

[1] *Assistant Professor, Ahsanullah University of Science and Technology, Bangladesh, Email: debasish.ce@aust.edu*
[2] *Corresponding Author, Associate Professor, Ahsanullah University of Science and Technology, Bangladesh, Email: fatema.ce@aust.edu*
[3] *Research Fellow, Housing and Building Research Institute, Bangladesh, Email: anikdas503@gmail.com*
[4] *Associate Professor, Okayama University, Japan, Email: hamood@okayama-u.ac.jp*
[5] *Senior Research Engineer, Housing and Building Research Institute, Bangladesh, Email: shafiulce@gmail.com*
[6] *Professor, Tohoku University, Japan, Email: maeda@archi.tohoku.ac.jp*
[7] *Research Fellow, Building Research Institute, Japan, Email: sekimatsutaro@yahoo.co.jp*
[8] *Professor, Chittagong University of Engineering & Technology, Bangladesh, Email: arbhuiyance@gmail.com*

that masonry infills generally improve lateral stiffness and strength, at least at low displacement demand and the growth of dissipated energy during ground motion. Therefore, an improvement in the lateral capacity by infill masonry can be considered during seismic evaluation of existing masonry infilled RC frames; however, the infill masonry walls are also the source of higher column shear demands and increased structural damage, which should be considered. It is to be noted that if infill masonry is not connected with surrounding RC members, the infill wall exhibits weak out-of-plane behavior, e.g., overturning of the infills [26]. The out-of-plane becomes more severe in cases where the slenderness of the infill is higher. Furthermore, the probability of overturning an infill wall is enhanced by the combination of the damage due to in-plane actions and the transverse acceleration demand during an earthquake. The level of destruction caused by the out-of-plane collapse is high, representing a significant risk for human life, safety, and economic losses [25]. Nevertheless, if the contribution of infill masonry is not sufficient to meet the seismic demand, then masonry infill can also be strengthened, which might improve both in-plane and out-of-plane behaviour. The infilled masonry walls of vulnerable RC buildings, based on seismic evaluation, can be strengthened by using different overlay or lamination schemes, e.g., Engineered Cementitious Composite (ECC), Textile Reinforced Mortar (TRM), Carbon Fiber Reinforced Polymer (CFRP), Fiber Reinforced Polymer (FRP), Ferrocement (FC), etc. Among these overlay schemes, FC strengthening is relatively easy and low-cost, when compared to other strengthening schemes, since FC strengthening can be conducted by utilizing only a mortar layer impregnated with wire mesh and necessary nail connections.

Several researchers investigated the lateral behavior of non-strengthened and ferrocement strengthened masonry infilled RC. From previous studies on masonry infilled RC frames [1-10], it is evident that masonry infills can improve lateral capacity and decrease deformation capacity when compared to bare RC frames. However, bending moments and shear demands, in turn, cause damage to the surrounding RC frame, depending on the flexibility of the RC frame with respect to infill masonry [27]. Meanwhile, from previous studies on ferrocement strengthened masonry infilled RC frames [1,28-32], it is evident that ferrocemnt strengthened masonry infill can improve lateral capacity and decrease deformation capacity when compared to that of masonry infilled RC frames. Although strengthening infill masonry walls with ferrocemnt can also change the shear demand and damage of RC frames, however, a comprehensive study is not available in the literature.

In this context, a comprehensive experimental program was designed to understand the effect of non-strengthened and ferrocemnt strengthened masonry infill on the behavior of the surrounding RC frame in terms of lateral strength, hinge formation on columns, shear demand enhancement, and damage to columns. In addition, the lateral strength of all the specimens was estimated considering the observed failure mechanism in the experimental program.

EXPERIMENTAL PROGRAM

Specimen Details

Three specimens, including a bare RC frame (BF), a masonry infilled RC frame (IM), and a ferrocement strengthened masonry infilled RC frame (IMFC), were designed to be aligned with the objectives of the current study. In all specimens, the RC frame had 180 mm square columns with 2.1% longitudinal reinforcement and a 180 x 300 mm top beam. RC columns were designed as flexural columns. 210 x 110 x 60 mm clay burnt bricks, commonly used in Bangladesh, were used to construct the masonry infill walls in the RC frame of the specimens IM and IMFC. The masonry walls were constructed after the curing of RC frames. Strengthening of the masonry wall of the specimen IMFC was conducted through several steps. After seven days of masonry construction, a 10 mm mortar layer was applied to both surfaces of the masonry infill wall, followed by mounting wire mesh on the mortar layer using nails, where nails were inserted into the wall with glue. Nails were spaced 250 mm and 500 mm in the horizontal and vertical directions, respectively. The nail spacing was considered in such a way that nine connections were available per square meter, as suggested by Alcocer and Flores [33] for confined masonry. The wire diameter and spacing of the wire mesh are given in Table 1. Finally, an additional 15 mm mortar layer was applied to the wire mesh. Therefore, the total thickness of ferrocement mortar was 25 mm on each surface of the masonry infill. The details of the specimens are shown in Figure 1(a) – (c). It is to be mentioned that the ferrocement layer has not been connected with the surrounding RC frame.

Table 1: Details of test specimens.

Specimen	RC column		Mas-onry	Ferro-cement		
	Dimension	Long. Reinf.	Thickness, t_{mas}	Thickness, t_{FC}	Wire dia., φ_{wm}	Wire spacing, s
	(mm)	-	(mm)	(mm)	(mm)	(mm)
BF	180 x 180	6-φ12mm	-	-	-	-
IM			110	-	-	-
IMFC			110	25	1	13

Material Properties

The average compressive strength of concrete was computed as 34.1 MPa as per ASTM C39 [34]. The yield strengths of longitudinal and transverse reinforcements, as presented in Table 2, were determined as per ASTM E8 [35]. The ultimate tensile strength of the wire mesh was 311.5 MPa. The average compressive strength and the average sliding strength of masonry were computed using masonry prisms and triplets, respectively. The prism test was conducted according to ASTM C1314 [36]. Since the obtained masonry compressive strength (i.e., 3.8 MPa) is less than the lower-bound unreinforced masonry strength, i.e., 6.9 MPa [37], the masonry used in this study has been considered low-strength masonry. The compressive strength of ferrocement mortar is 9.42 MPa.

Table 2: Material properties.

Material	Strength (MPa)	
Concrete	Compressive strength (28 days)	34.12
Steel (yield strength)	Long reinforcement (12mm-φ)	545
	Shear reinforcement (8mm-φ)	630
Masonry	Prism compressive strength	3.80
	Sliding strength	0.07
Ferro cement	Mortar compressive strength	9.42

Instrumentation and Loading Protocol

The specimens were mounted on a steel rig, as shown in Figure 2, situated at Housing and Building Research Institute (HBRI), Bangladesh. The displacements at the mid-height of the top beam, both on the front and back sides, were recorded

using the LVDTs (LVDT 3, 4, 5, and 6) shown in Figure 2. The average of all displacements was used to compute the story drift. The slip at the top joint (i.e., the interface of the top of the infill wall and the top beam soffit) was recorded using an LVDT (LVDT-2) mounted on the back side of the top beam, as shown in Figure 2. Meanwhile, an LVDT (LVDT-1) was mounted on the steel rig, as shown in Figure 2, to check the slip at the base. The specifications of all LVDTs used in this study are given in Annexure A1. In addition, several strain gauges were mounted on longitudinal and transverse reinforcements of the columns of specimens, as shown in Figure 1(a), to record strain values at different drift levels. All specimens were subjected to a quasi-static cyclic lateral load using two jacks, as shown in Figure 2, considering the loading protocol shown in Figure 3, where two cycles of each story drift were applied.

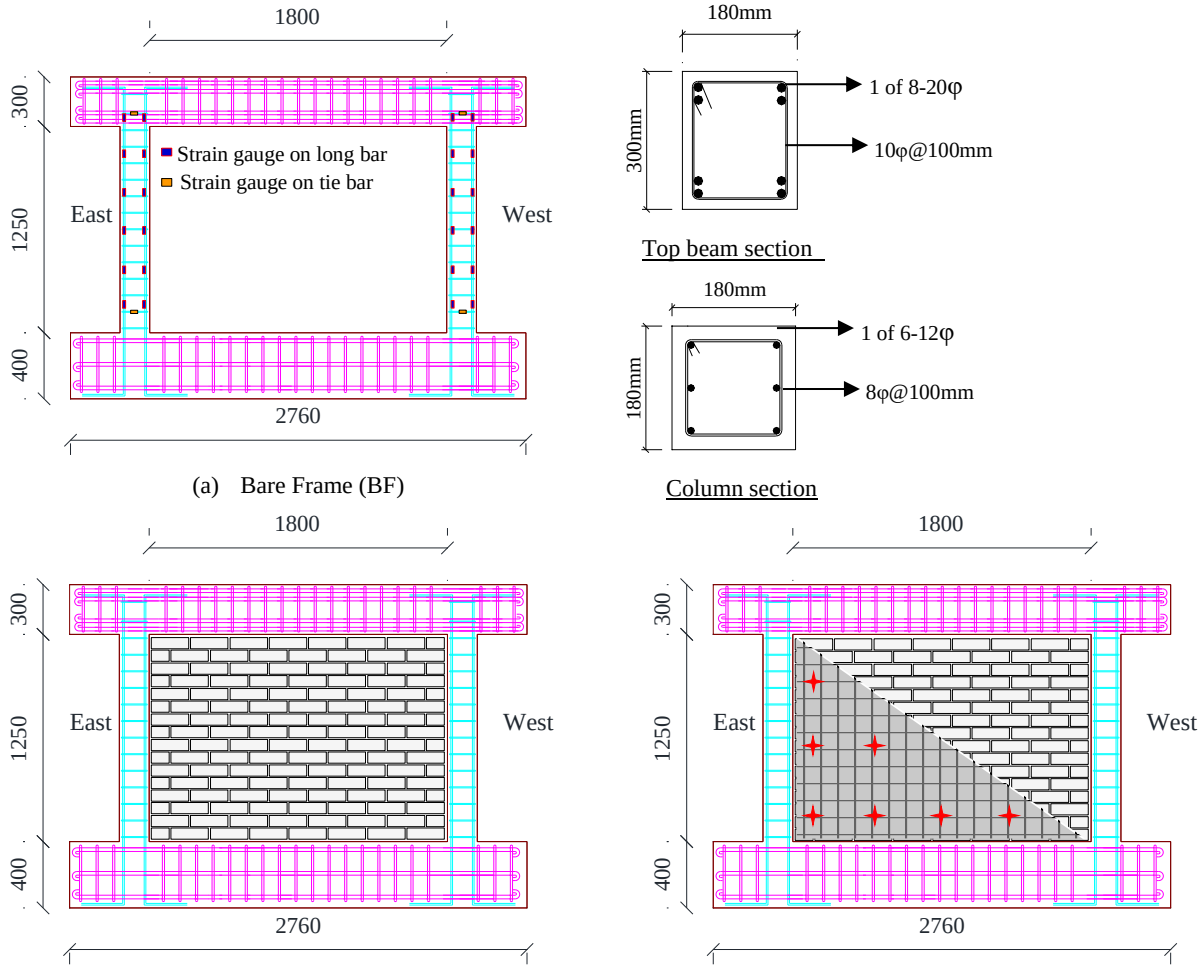

Figure 1: Details of specimens (a) Bare RC frame (BF), (b) Masonry infilled RC frame (IM), and (c) Ferrocement strengthened masonry infilled RC frame (IMFC) (all dimensions are in "mm").

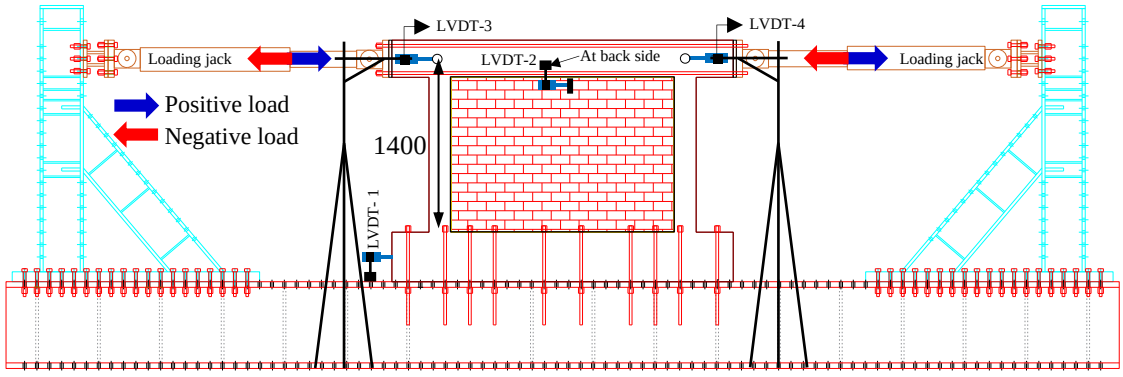

Note: **LVDT-1**: slip at base; **LVDT-2**: slip at top joint; **LVDT-3**, **4**, **5**, **6**: story displacement at the center of beam-column joint of both front and back sides.

Figure 2: Schematic diagram of the LVDT setup and specimen loading.

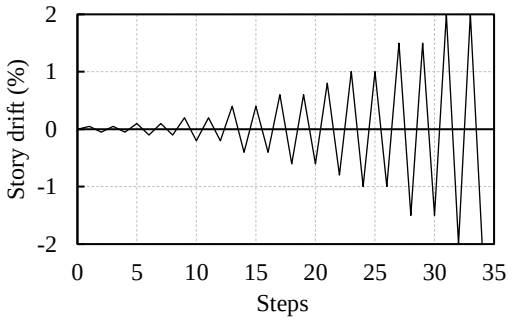

Figure 3: Loading protocol for the test specimens.

Bare RC Frame (BF)

The hysteresis behavior of the bare RC frame (BF) is shown in Figure 4(a). It behaved essentially in an elastic manner at the lower drift levels. Several flexural cracks appeared at the bottom of the tension column at about 0.1% story drift. After that, new flexural cracks appeared at the top of the tension column, and the bottom of the compression column at 0.2%, and 0.4% story drifts, respectively. Longitudinal reinforcement at the bottom of the tension column yielded at 0.6% story drift, which was observed from recorded strain values. After long reinforcement yielding, the RC frame showed non-linear behavior as portrayed in Figure 4(a). Several shear cracks appeared on the beam-column joint at about 0.8% story drift,

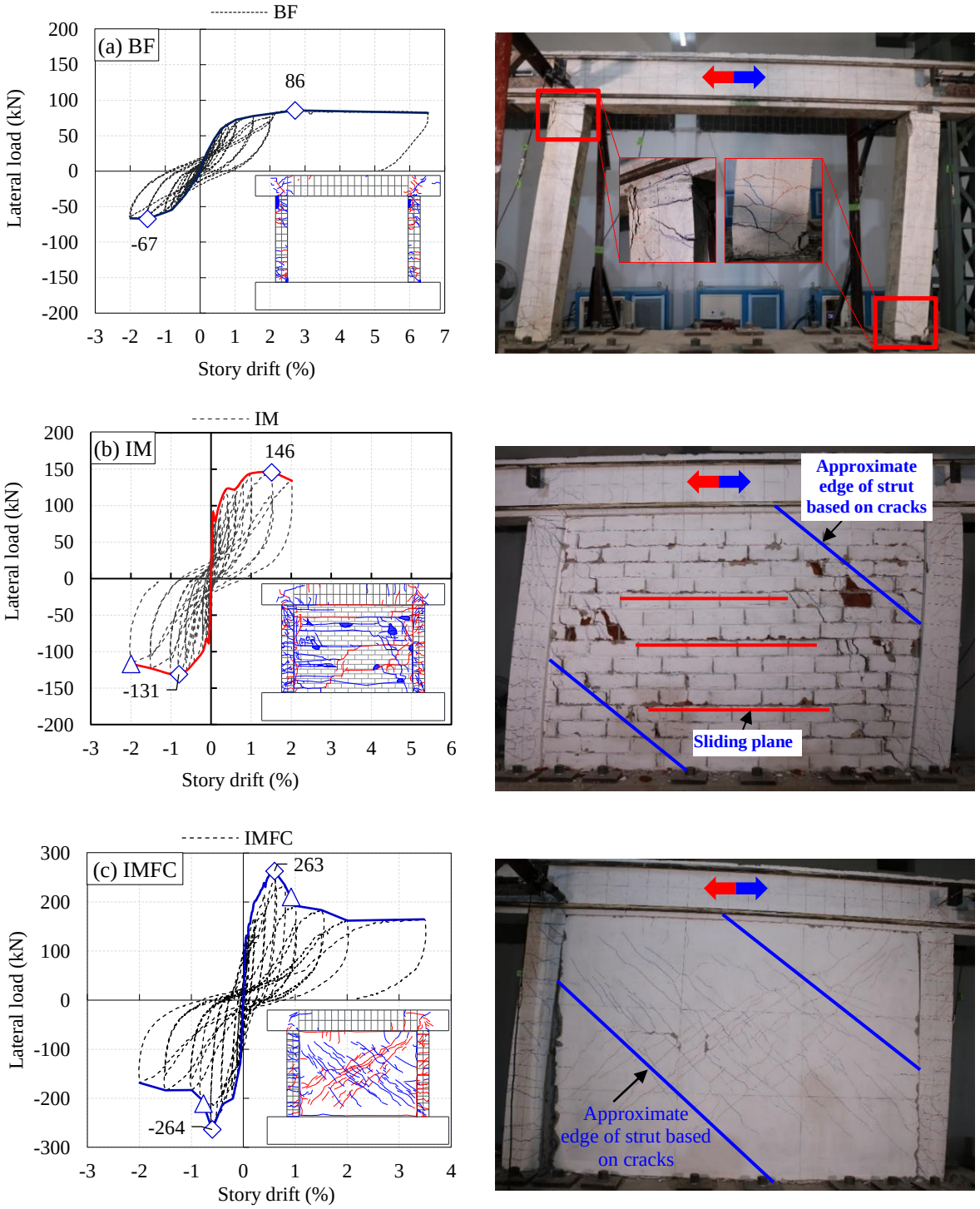

Figure 4: Lateral load-story drift relationship and final damage state of (a) Bare RC frame (BF), (b) Masonry infilled RC frame (IM), and (c) Ferrocement strengthened masonry infilled RC frame (IMFC).

however, crack size was not significant, i.e., less than 0.2 mm. Following these damages, several cracks appeared on both columns in between 1% to 1.5% story drifts. The RC frame showed maximum resistance of 86 kN and -67 kN at about 2.7% and -1.5% story drift, respectively. After 2% story drift, the specimen was pushed monotonically up to 6.5% story drift in the positive direction and the frame sustained the resistance without notable capacity degradation. The final damage is shown on the right side of Figure 4(a).

EXPERIMENTAL OBSERVATION

Masonry Infilled RC frame (IM)

The hysteresis behavior of the masonry infilled RC frame (IM) is shown in Figure 4(b). Several flexural cracks appeared at the mid-height of the tension column at about 0.05% story drift. It is to be noted that under positive lateral loading (i.e., from the left to the right of the frame), the left and right columns are termed as the tension column and the compression column, respectively. After that, a horizontal crack formed at the mid-height of the infill masonry at 0.1% drift. At 0.2% drift, some new flexural cracks appeared on the tension column. At 0.4% to 0.6% story drift, new shear cracks appeared at the top of the tension column, and new horizontal and diagonal cracks appeared on the infill masonry. Longitudinal reinforcement at the mid-height of the tension column yielded at about 0.8% story drift, which was observed from recorded strain values. The masonry infilled RC frame showed a maximum lateral resistance of 146 kN and -131 kN at 1.5% and -0.8% story drifts, respectively. At 2% story drift, the lateral loading was stopped. The final damage is shown on the right side of Figure 4(b). Sliding of the infill masonry was the main resistance mechanism of the infill wall, where the edge of the diagonal strut is evident based on the cracks shown in Figure 4(b). The final failure mechanism can be idealized as a knee-braced frame model for sliding failure of masonry infill as described by Paulay and Priestley [38], where the vertical component of the diagonal strut force acts as a clamping force across the sliding surfaces. Since infill masonry is susceptible to out-of-plane failure, the out-of-plane capacity degradation of the non-strengthened masonry infill subjected to different in-plane story drifts, using an analytical model suggested by Abrams et al. [39], is discussed separately in Annexure A2.

Ferrocement Strengthened Masonry Infilled RC Frame (IMFC)

The hysteresis behavior of the ferrocement strengthened masonry infilled RC frame (IMFC) is shown in Figure 4(c). Several flexural cracks appeared on the full height of the tension column at about 0.05% story drift, which was followed by a horizontal crack at the base of the ferrocement strengthened masonry infill at 0.1% drift. At 0.2% drift, a shear crack appeared at the top of the tension column. At 0.4%, a diagonal crack appeared at the center of the strengthened wall, which indicates the formation of a diagonal strut. In the subsequent story drift, i.e., 0.6% story drift, several diagonal cracks appeared on the wall and propagated to the loading corner. The longitudinal reinforcement at the bottom of the tension column yielded at 0.6% story drift, which was observed from the recorded strain value. The strengthened masonry infilled frame showed maximum resistance of 263 kN and -264 kN at about 0.6% and -0.6% story drift, respectively. At 0.8% story drift, delamination of the ferrocement layer was observed near the bottom of the compression column. After that, the lateral resistance degraded by about 20% at around 1.0% story drift. After 2% story drift, the specimen was pushed monotonically up to 3.5% and stopped due to safety concerns. The final damage is shown on the right side of Figure 4(c).

EFFECT OF INFILL WALL ON THE BEHAVIOR OF SURROUNDING RC FRAME

Lateral Strength and Ductility

The backbone curves of all the specimens are shown in Figure 5. The bare frame specimen showed ductile behavior with a maximum resistance of 77 kN (an average of positive and negative loading). Insertion of non-strengthened masonry improved the lateral capacity, on average, by 81%, whereas the deformation capacity was reduced. Meanwhile, the insertion of ferrocement strengthened masonry infill enhanced the lateral strength, on average, by 244% and 90% when compared to the lateral strength of the bare frame and masonry infilled RC frame, respectively. However, the average deformation capacity of the specimen IMFC (i.e., 0.6% story drift) was 33% less than the average deformation capacity of the specimen IM (i.e., 0.9%) at the peak resistance. The lower deformation capacity can be attributed to the presence of the relatively rigid masonry infill wall with ferrocement lamination.

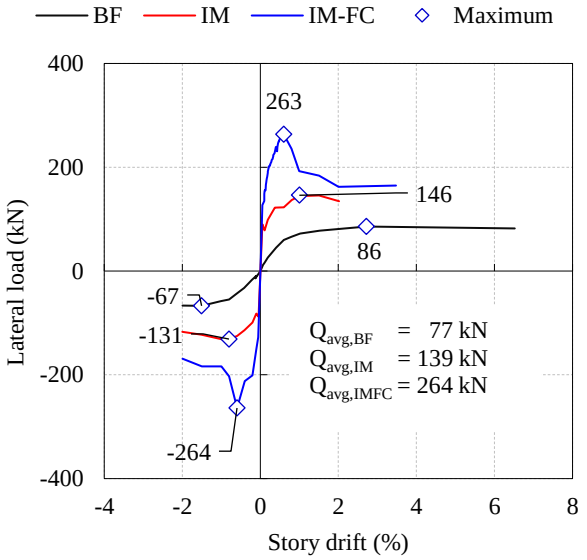

Figure 5: Backbone curves of the test specimens.

Hinge Formation on Columns

The curvature distribution along the height of the column and the location of plastic hinges are shown in Figure 6(a)-(c) considering the positive loading. The tension and compression columns (as defined in Section 3.2) are shown on the left and right sides of Figure 6, respectively. The curvature (φ) at a certain height of a column has been estimated using the strains recorded by two strain gauges affixed to the tensile and compression longitudinal bars at that level using Equation 1. It is important to mention that clockwise rotation has been considered as positive.

$$\varphi = \frac{\varepsilon_t - \varepsilon_c}{l} \quad (1)$$

where, ε_t = strain of tensile reinforcement, ε_c = strain of compression reinforcement, and l = center-to-center distance of longitudinal reinforcements.

The location of the plastic hinges has been estimated considering the largest value of curvature, i.e., rotation per unit length. For the bare frame specimen (BF), rotation was concentrated on the top and bottom of the tension and compression columns, as shown in Figure 6(a), which resembles the visual cracks and damages at the same locations, as shown in the final damage of the bare frame in Figure 4(a).

Therefore, plastic hinges formed at the top and bottom of both columns as the columns were designed as flexural columns. In the case of the masonry infilled RC frame (IM), rotation was concentrated at the top and mid-height of the tension column, as shown in Figure 6(b). The mid-height plastic hinge formation resembled the initial flexural crack formation at the mid-height of the tension column due to the horizontal cracking on the masonry infill. However, the rotations were concentrated at the top and bottom of the compression column. Therefore, a short column was formed in the tension column, whereas plastic hinges were formed at the top and bottom of the compression column. In the case of the strengthened masonry infilled RC frame (IMFC), rotation was concentrated at the top and bottom of the tension and compression columns, as shown in Figure 6(c). Therefore, the locations of the plastic hinges are similar to those of the bare frame specimen (BF). Therefore, the application of ferrocement to low-strength masonry eliminated the short-column phenomenon by improving the shear capacity of the infill masonry.

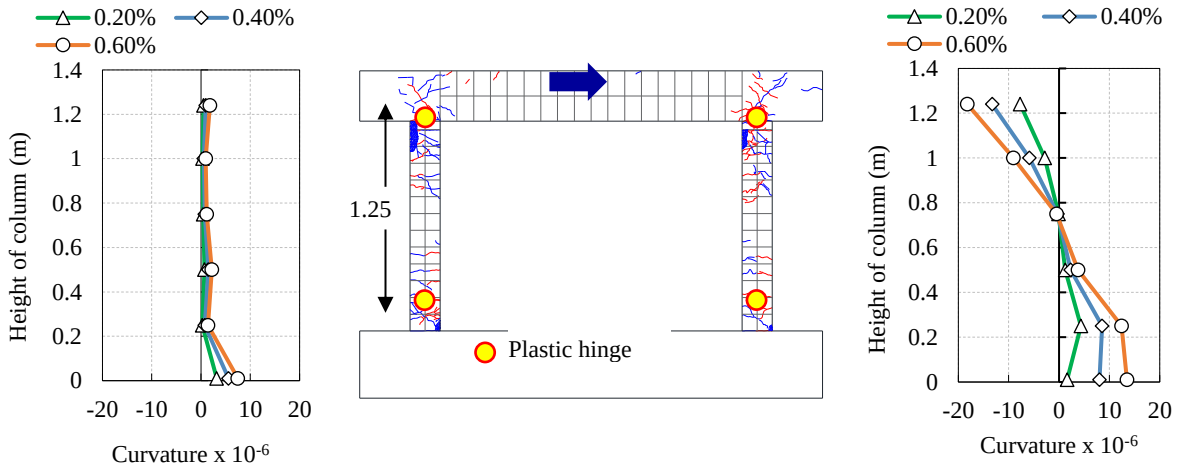

(a) Bare Frame (BF)

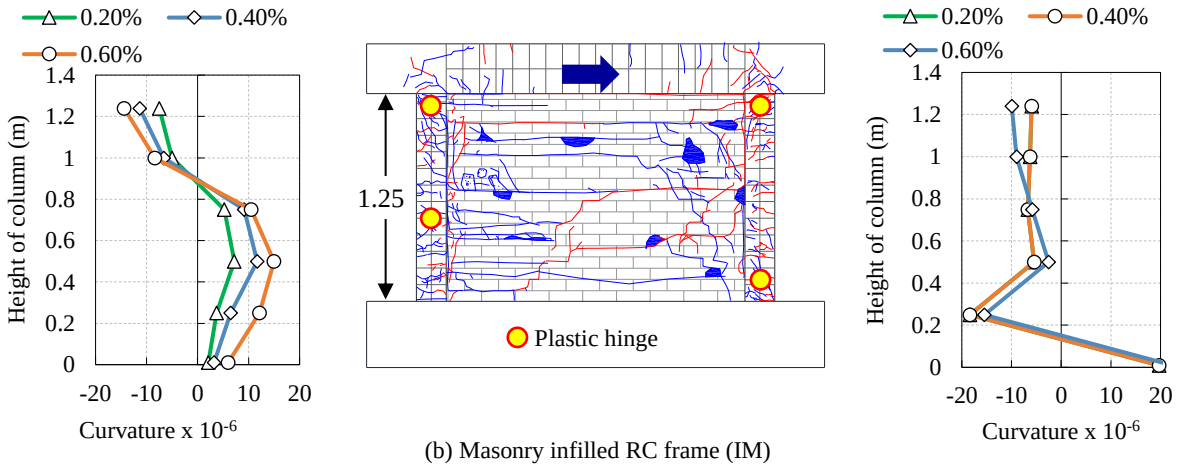

(b) Masonry infilled RC frame (IM)

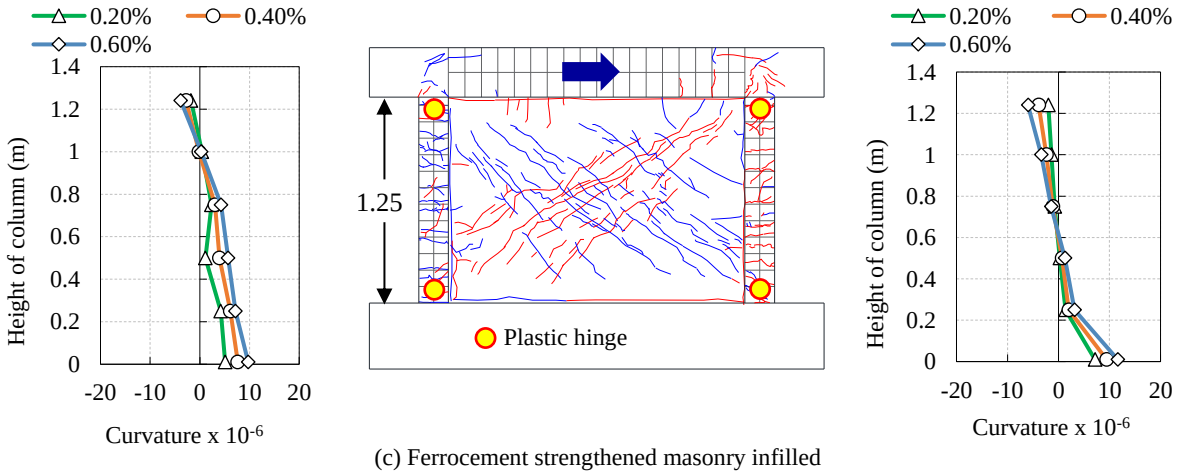

(c) Ferrocement strengthened masonry infilled RC frame (IMFC)

Figure 6: Curvature of tension and compression column and location of hinges of (a) Bare RC frame (BF), (b) Masonry infilled RC frame (IM), and (c) Ferrocement strengthened masonry infilled RC frame (IMFC) (clockwise rotation is positive).

Shear Demand Enhancement

Generally, infill walls increase the shear demand of the RC column [11-15] in the region adjacent to the loaded corner, as illustrated in Figure 7. The shear demand enhancement due to the non-strengthened and ferrocement strengthened masonry infill is discussed in this section. The slip at the interface of the infill wall and top beam soffit, and the strain on shear reinforcement at the top of the tension column have been investigated to understand the shear demand.

The slip at the interface of the beam soffit and top of the infill wall of specimens, recorded using LVDT, is shown in Figure 8. The slip observed in the specimen IM was relatively less compared to the slip observed in the test specimen IMFC. The lower slip at the top interface in the test specimen IM can be attributed to the phenomenon that the non-strengthened masonry infill can slide along several mortar joints, i.e., several mortar joints of masonry are susceptible to failing under sliding (as observed in Figure 4(b)). These multiple sliding movements helped the non-strengthened masonry to accommodate in the deformed RC frame, which can reduce the slip at the top interface. On the other hand, when ferrocement is applied to the masonry wall, those weaker mortar joints might have an enhanced shear capacity due to the presence of wire mesh in the ferrocement mortar layer, keeping the top masonry joint with beam soffit as weak as before since the wire mesh was not connected to the RC frame. Therefore, all the sliding movements might be concentrated at that joint, which is evident in this study, i.e., more slip concentrated at the top joint, as shown in Figure 8, in the case of the test specimen IMFC. The enhanced slip at the top joint may increase the shear demand at the top of the tension column of the specimen IMFC when compared to the specimen IM. In this context, the recorded strain of the top tie reinforcement is shown in Figure 9. It is evident that the strain demand at the top of the tension column increased in the cases of masonry infilled RC frame (IM) and ferrocement strengthened masonry infilled RC frame (IMFC) specimens when compared to the bare frame (BF). In the case of specimen IMFC, the slip at the top is higher, as shown in Figure 8, and the initial strain of the tie bar is higher, as illustrated in Figure 9. The higher initial strain on the tie bar might be due to the early formation of the diagonal strut. However, there was a sudden drop in the tie strain after 0.6% story drift, which can be attributed to the crack opening on the ferrocement strengthened infill wall, from 0.6% to 1.0% story drift, as shown in the close view of Figure 9. It is to be noted that tie reinforcement did not yield in any specimen, i.e., tie strains were less than the yield strain, ε_y = 2000μ, as shown in Figure 9.

By comparing the tie strains at the top of the tension column of the specimens IM and IMFC, it can be summarized that the tie strain (which indirectly represents shear demand due to abutting the infill wall) enhancement due to ferrocement lamination is not that much when compared to the non-strengthened masonry infilled specimen (IM). Therefore, shear demand enhancement due to the ferrocement lamination used in this study is not substantial when compared to the non-strengthened specimen (IM).

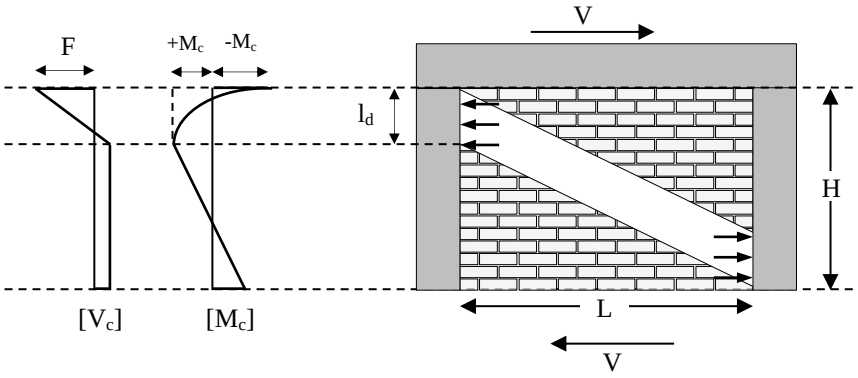

Figure 7: Influence of infill wall on RC columns' local demand (redrawn from Dias-Oliveira et al. [40]).

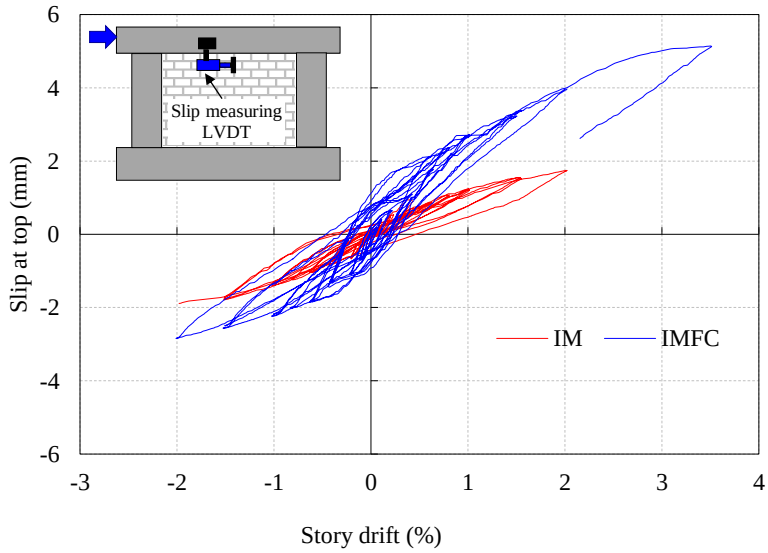

Figure 8: Slip at the interface of the top masonry layer and top beam soffit non-strengthened (IM) and Ferrocement strengthened masonry (IMFC) infilled RC frame.

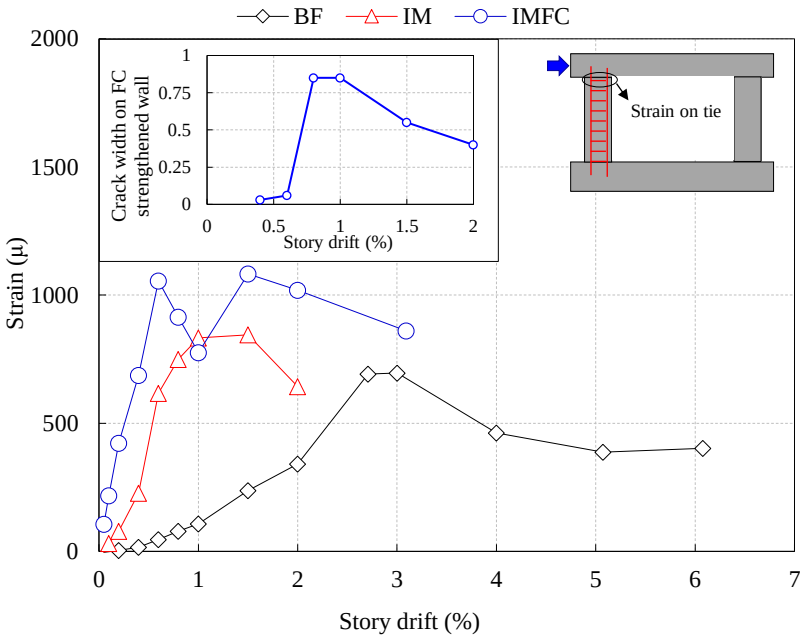

Figure 9: Tie reinforcement's strain at the top of the tension column (yield strain, ε_y = 2000μ).

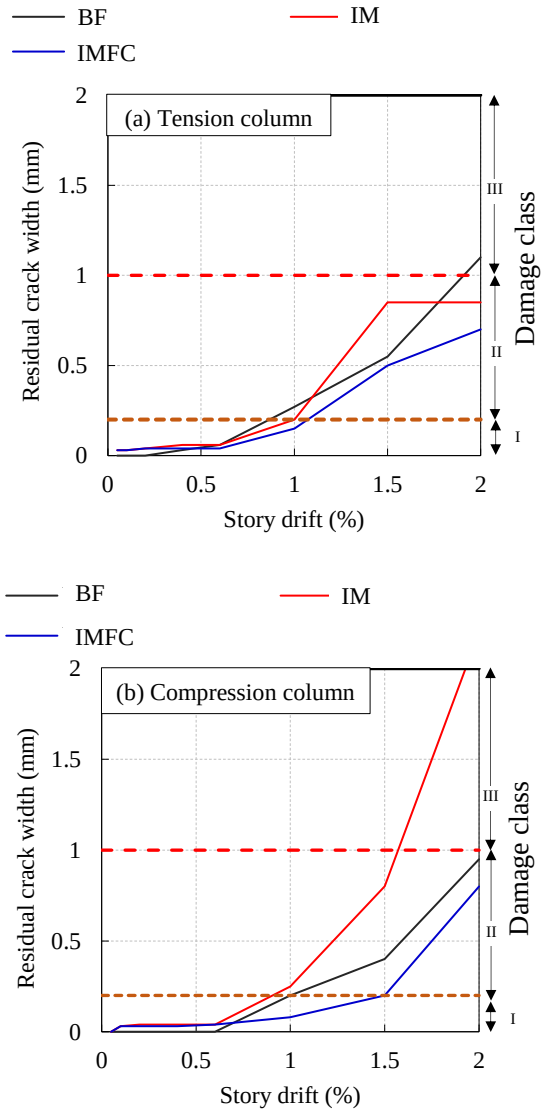

Figure 10: Residual crack width of (a) Tension column and (b) Compression column of the test specimens.

Table 3: Damage classes of RC elements (Japanese standard of post-earthquake damage evaluation [41]).

Damage class	Description of damage
I	• Visible narrow cracks on concrete surface (Crack width is less than 0.2 mm)
II	• Visible clear cracks on concrete surface (Crack width is about 0.2 ~ 1.0 mm)
III	• Local crush of covering concrete • Remarkable wide cracks (Crack width is about 1.0 ~ 2.0 mm)
IV	• Remarkable crush of concrete with exposed reinforcing bars • Spalling off of covering concrete (Crack width is more than 2.0 mm)
V	• Buckling of reinforcing bars • Cracks in core concrete • Visible vertical deformation in columns and/or walls • Visible settlement and/or inclination of the building

Damage to Columns

Damage to columns has been considered in terms of residual crack sizes measured after the unloading of specimens at each loading cycle. The residual crack widths of the tension and compression columns of all the test specimens for the first cycle of positive loading are shown in Figure 10. The damage class of reinforced concrete has been considered as defined in Table 3 by Japanese standard for post-earthquake damage evaluation [41]. The tension and compression columns of the bare frame showed damage level-II up to 2% story drift. In the case of the non-strengthened masonry infilled RC frame (IM), the tension column showed damage level-II up to 2% story drift, whereas the compression column showed more damage (i.e., damage level-III ~ IV) due to the shear cracking at the bottom of the compression column. In the case of the strengthened masonry infilled RC frame (IMFC), the tension column showed similar

damage as the bare frame and non-strengthened masonry specimens up to 2% story drift, whereas the compression column showed less damage (i.e., damage level-II). Less damage to the compression column might be attributed to the delamination of the ferrocement mortar layer that occurred at the bottom near the compression column. In other words, if delamination did not occur, more strut forces would act on the compression column, which might cause more damage. By comparing the crack widths of tension and compression columns of all the specimens, as shown in Figure 10, it is clear that the damage to RC columns changed to a smaller extent after the insertion of both non-strengthened and ferrocement strengthened masonry infill when compared to the damage to the columns of the RC bare frame. The measured damages, i.e., residual crack widths of the columns, were within 1.0 ~ 2.0 mm.

LATERAL STRENGTH EVALUATION

In this section, the lateral strength capacities of tested specimens have been computed considering the lateral strength estimation models that idealized the observed failure mechanisms. The computed lateral strengths have also been compared with the experimental lateral strengths.

Strength Prediction Models

Bare Frame (BF)

Bare frame capacity has been evaluated considering the flexural hinge formation at the top and bottom of the frame, as shown in Figure 11(a), which resembles the experimental observation. The moment capacity of the top hinge has been considered as the minimum capacity of the beam and column. The lateral capacity can be calculated as per Japanese seismic evaluation guidelines [42], using Equation 2 to Equation 3.

$$Q_{BF} = 2 \text{ x } Q_{mu} \tag{2}$$

$$Q_{mu} = \frac{M_{u,t}+M_{u,b}}{h_o} \tag{3}$$

where, Q_{BF} = RC frame capacity, Q_{mu} = shear demand of the column at flexural yielding, $M_{u,t}$ = minimum of the ultimate moment capacities of beam and column at the top joint, $M_{u,b}$ = ultimate moment capacity of column, and h_o = clear height of the column.

Masonry Infilled RC Frame (IM)

The lateral capacity of the masonry infilled RC frame has been computed considering the failure mechanism idealized as a knee-braced frame model for sliding failure of masonry infill [38] where the vertical component of the diagonal strut force acts as a clamping force across the sliding surfaces as shown in Figure 11(b). The clamping force also contributes to the sliding capacity of the infill masonry, and the sliding capacity is presented in Equation 4 proposed by Paulay and Priestley [38]. The lateral capacity of the RC frame has been computed as per Equation 5 considering the plastic hinge locations shown in Figure 11(b). The total lateral capacity of specimen IM has been computed using Equation 6.

$$\tau_{mas} = \frac{0.03 f_m}{1-0.3\cdot\frac{h_{inf}}{l_{inf}}} \tag{4}$$

$$Q_{FR,IM} = \frac{M_{u,t}+M_{u,b}}{h_1} + \frac{M_{u,t}+M_{u,b}}{h_o} \tag{5}$$

$$Q_{IM} = Q_{FR,IM} + \tau_{mas} \cdot t_{inf} \cdot l_{inf} \tag{6}$$

where, τ_{mas} = shear strength of masonry, f_m= compressive strength of masonry, h_{inf}, t_{inf}, l_{inf} = height, thickness and length of infill masonry, $Q_{FR,IM}$ = RC frame capacity, $M_{u,t}$ = minimum of the ultimate moment capacities of beam and column at top joint, $M_{u,b}$ = ultimate moment capacity of column, h_o = clear height of compression column, h_1 = half height of tension column, and Q_{IM} = lateral capacity of masonry infilled RC frame.

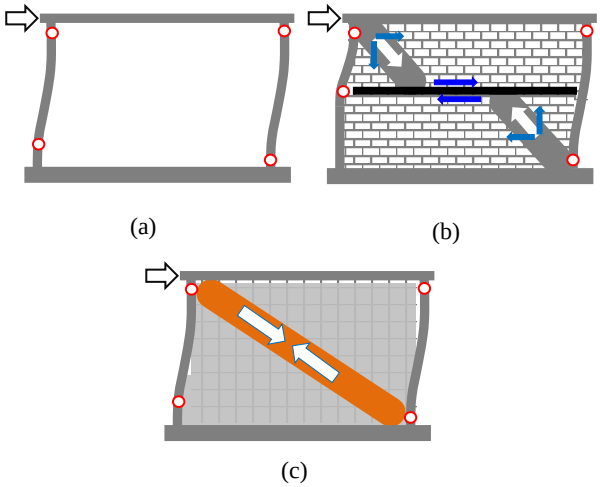

Figure 11: Idealized failure mechanism of (a) Bare RC frame (BF), (b) Masonry infilled RC frame (IM), and (c) Ferrocement strengthened masonry infilled RC frame (IMFC).

Ferrocement Strengthened Masonry Infilled RC Frame (IMFC)

The schematic diagram of the observed failure mechanism of the FC strengthened masonry infilled RC frame is shown in Figure 11(c). The ferrocement strengthened masonry infill cracked on the loaded diagonal direction, whereas the frame behaves like the bare frame, i.e., hinges at the top and bottom of columns. The lateral capacity of the observed failure has been evaluated by Equation 7. The lateral strength of the RC frame (Q_{BF}) has been computed by Equation 2 as discussed in the earlier subsection. The strut width (W_s) of ferrocement strengthened masonry infill has been considered based on the relative stiffness of the RC frame and ferrocement strengthened masonry wall, as suggested by Sen et al. [43].

$$Q_{IMFC} = Q_{BF} + \left(0.5 f_{m,90} W_s t_{mas} + 0.5 f_{mor,FC} W_s n_s t_{FC}\right) Cos\theta \tag{7}$$

where, $f_{m,90}$ = expected prism compressive strength of masonry in horizontal direction (= 0.5 *x* masonry prism compressive strength, f_m), $f_{mor,FC}$ = FC mortar compressive strength, W_s = strut width of ferrocement strengthened masonry infill, t_{mas}, t_{FC} = thickness of masonry and FC mortar layer, n_s = number of surface retrofitted with FC, and θ = inclination of loaded diagonal with horizontal.

Comparison between Experimental and Estimated Lateral Strength

The experimental and estimated lateral strengths of the test specimens, along with the idealized failure mechanism, are presented in Table 4. The experimental to estimated lateral strength ratio varies within 0.9 to 1.0, which indicates a fair performance of the considered lateral strength prediction models.

Table 4: Comparison of experimental and estimated lateral strengths.

Specimen (Idealized failure mechanism)	Contribution of different components			Lateral strength (kN)		
	RC frame	Masonry infill	Ferro cement layer	Estimated, $Q_{est.}$	Experimental, $Q_{exp.}$ (positive loading)	$Q_{exp.}/Q_{est.}$
BF [Figure 11(a)]	85.2	-	-	85.2	86	1.00
IM [Figure 11(b)]	135.5*	25.9	-	161.4	146	0.90
IMFC [Figure 11(c)]	85.2	61.8	139.3	286.3	263	0.92

* Considering plastic hinge at mid-height of tension column

CONCLUSIONS

This study aimed to investigate the effect of non-strengthened and ferrocement strengthened masonry infill on the behavior of the surrounding RC frame in terms of lateral strength, hinge formation on columns, shear demand enhancement, and damage to columns. In addition, the estimation of the lateral strength of all the specimens was conducted considering the observed failure mechanism in the experimental program. The concluding remarks within the limited scope of this study are:

- Non-strengthened and ferrocement strengthened masonry walls increased the lateral strength of the RC frame, on average, by 81% and 244%, respectively, when compared to the lateral strength of the bare RC frame. At the same time, ferrocement strengthening improved the lateral strength, on average, by 90% when compared with that of the masonry infilled RC frame.
- Insertion of low-strength masonry triggered the short column formation following the horizontal crack in the infill masonry. However, an application of ferrocement to low-strength masonry improved the in-plane shear capacity of the infill masonry, which in turn eliminated the short-column formation. In other words, the failure mechanism changed from the sliding failure to the diagonal compression failure.
- The shear demand of the tension column of the ferrocemment strengthened masonry infilled RC frame was not substantial, as observed by strains on tie reinforcements, when compared to that of the non-strengthened masonry infilled RC frame.
- Damage concentration on RC columns changed to a smaller extent, where residual crack widths were within 1.0 ~ 2.0 mm, after the insertion of the non-strengthened and strengthened masonry infill.
- The lateral capacity of the bare frame, non-strengthened, and ferrocement strengthened masonry infilled RC frame has been estimated based on the idealization of the observed failure mechanisms. The experimental to estimated lateral strength ratio varies within 0.9 to 1.0, which indicates a fair performance of the considered lateral strength estimation models.

ACKNOWLEDGMENTS

This research is supported and funded by JICA through SATREPS–TSUIB project (principle investigators: Prof. Yoshiaki Nakano, U. Tokyo and Mr. Md Ashraful Alam, HBRI, Bangladesh). The experimental work has been conducted in Earthquake Laboratory, Housing and Building Research Institution (HBRI), Dhaka, Bangladesh. Hence authors extend their thanks to all of the staffs of SATREPS–TSUIB project, especially Mr. Malek Sikder, Senior Consultant of the Project. A special thanks to Prof. Dr. Sharmin Reza Chowdhury, Dr. Fatema-Tuz-Zahura, Ms. Zasiah Tafheem, and Mr. Munirul Islam for their cordial cooperation in the research project.

REFERENCES

1 Seki M, Popa V, Lozinca E, Dutu A and Papurcu A (2018). "Experimental study on retrofit technologies for RC frames with infilled brick masonry walls in developing countries". *Proceedings of the 16th European Conference on Earthquake Engineering*, Romania.

2 Suzuki T, Choi H, Sanada Y, Nakano Y, Matsukawa K, Paul D and Binici B (2017). "Experimental evaluation of the in-plane behaviour of masonry wall infilled RC frames". *Bulletin of Earthquake Engineering*, **15**: 4245-4267. https://doi.org/10.1007/s10518-017-0139-1

3 Basha SH and Kaushik HB (2012). "Evaluation of shear demand on columns of masonry infilled reinforced concrete frames". *Proceedings of the 15th World Conference on Earthquake Engineering*, Lisbon, Portugal.

4 Stylianidis KC (2012). "Experimental investigation of masonry infilled R/C frames". *The Open Construction & Building Technology Journal*, **6**(1): 194-212. http://dx.doi.org/10.2174/1874836801206010194

5 Stavridis A (2009). "*Analytical and experimental study of seismic performance of reinforced concrete frames infilled with masonry walls"*. PhD Dissertation, University of California, San Diego.

6 Murty CVR and Jain SK (2000). "Beneficial influence of masonry infill walls on seismic performance of RC frame buildings". *Proceedings of the 12th World Conference on Earthquake Engineering*, Auckland, New Zealand.

7 Chiou YJ, Tzeng JC and Liou YW (1999). "Experimental and analytical study of masonry infilled frames". *Journal of Structural Engineering*, **125**(10): 1109-1117. https://doi.org/10.1061/(ASCE)0733-9445(1999)125:10(1109)

8 Al-Chaar GK (1998). "*Nonductile behavior of reinforced concrete frames with masonry infill panels subjected to in-plane loading"*. PhD Dissertation, University of Illinois at Chicago.

9 Mehrabi AB, Benson SP, Schuller MP and Noland JL (1996). "Experimental evaluation of masonry-infilled RC frames". *Journal of Structural Engineering*, **122**(3): 228-237. https://doi.org/10.1061/(ASCE)0733-9445(1996)122:3(228)

10 Leuchars JM and Scrivener JC (1976). "Masonry infill panels subjected to cyclic in-plane loading". *Bulletin of the New Zealand Society for Earthquake Engineering*, **9**(2): 122-131. https://doi.org/10.5459/bnzsee.9.2.122-131

11 Di Trapani F, Bogatkina V, Petracca M and Camata G (2023). "Evaluation of the additional shear demand due to frame-infill interaction: a new capacity model". *Procedia Structural Integrity*, **44**, 496-503. https://doi.org/10.1016/j.prostr.2023.01.065

12 Kim M and Yu E (2021). "Experimental study on lateral-load resisting capacity of masonry-infilled reinforced concrete frames". *Applied Sciences*, **11**(21): 9950. https://doi.org/10.3390/app11219950

13 Milanesi RR, Morandi P and Magenes G (2018). "Local effects on RC frames induced by AAC masonry infills through FEM simulation of in-plane tests". *Bulletin of Earthquake Engineering*, **16**: 4053-4080. https://link.springer.com/article/10.1007/s10518-018-0353-5

14 Maidiawati and Sanada Y (2017). "R/C frame–infill interaction model and its application to Indonesian buildings". *Earthquake Engineering and Structural Dynamics*, **46**(2): 221-241. https://doi.org/10.1002/eqe.2787

15 Cavaleri L and Di Trapani F (2015). "Prediction of the additional shear action on frame members due to infills". *Bulletin of Earthquake Engineering*, **13**: 1425-1454. https://doi.org/10.1007/s10518-014-9668-z

16 Srechai J, Wararuksajja W, Leelataviwat S and Limkatanyu S (2023). "Performance evaluation of low-rise infilled reinforced concrete frames designed by considering local effects on column shear demand". *Frontiers of Structural and Civil Engineering*, **17**: 686-703. https://doi.org/10.1007/s11709-023-0937-2

17 Wararuksajja W, Srechai J, Leelataviwat S, Sungkamongkol T and Limkatanyu S (2021). "Seismic design method for preventing column shear failure in reinforced concrete frames with infill walls". *Journal of Building Engineering*, **44**: 102963. https://doi.org/10.1016/j.jobe.2021.102963

18 Brzev S, Pandey B, Maharjan DK and Ventura C (2017). "Seismic vulnerability assessment of low-rise reinforced concrete buildings affected by the 2015 Gorkha, Nepal, earthquake". *Earthquake Spectra*, **33**: 275-298. https://doi.org/10.1193/120116eqs218m

19 Pokharel T and Goldsworthy HM (2017). "Lessons learned from the Nepal earthquake 2015". *Australian Journal of Structural Engineering*, **18**(1): 11-23. https://doi.org/10.1080/13287982.2017.1309818

20 Dizhur D, Dhakal RP, Bothara J and Ingham JM (2016). "Building typologies and failure modes observed in the 2015 Gorkha (Nepal) earthquake". *Bulletin of the New Zealand Society for Earthquake Engineering*, **49**(2): 211-232. https://doi.org/10.5459/bnzsee.49.2.211-232

21 Adhikari RK, Bhagat S and Wijeyewickrema AC (2015). "Damage scenario of reinforced concrete buildings in the 2015 Nepal earthquakes". *14th International Symposium on New Technologies for Urban Safety of Mega Cities in Asia*, Kathmandu, Nepal, 29-31.

22 Augenti N and Parisi F (2010). "Learning from construction failures due to the 2009 L'Aquila, Italy, earthquake". *Journal of Performance of Constructed Facilities*, **24**(6): 536-555. https://doi.org/10.1061/(ASCE)CF.1943-5509.0000122

23 Hopkins D, Bell D, Benites R, Burr J, Hamilton C and Kotze R (2008). "The Pisco (Peru) earthquake of 15 August 2007: NZSEE reconnaissance report, June 2008". *Bulletin of the New Zealand Society for Earthquake Engineering*, **41**(3): 109–192. https://doi.org/10.5459/bnzsee.41.3.109-192

24 Van de Vorstenbosch G, Charleson AW and Dowrick DJ (2002). "Reinforced concrete building performance in the Mw 7.8 1931 Hawke's Bay, New Zealand, earthquake". *Bulletin of the New Zealand Society for Earthquake Engineering*, **35**(3): 149-164. https://doi.org/10.5459/bnzsee.35.3.149-164

25 Furtado A, Rodrigues H, Arêde A and Varum H (2021). "A review of the performance of infilled RC structures in recent earthquakes". *Applied Sciences*, **11**(13): 5889. https://doi.org/10.3390/app11135889

26 Çetin KÖ and Ilgaç M (2023). "*Reconnaissance Report on February 6, 2023 Kahramanmaraş-Pazarcık (Mw=7.7) and Elbistan (Mw=7.6) Earthquakes"*. Türkiye Earthquake Reconnaissance and Research Alliance.

27 Crisafulli FJ (1997). "*Seismic behaviour of reinforced concrete structures with masonry infills"*. PhD Dissertation, University of Canterbury, New Zealand.

28 Sen D, Alwashali H, Islam MS, Seki M and Maeda M (2023). "Lateral strength evaluation of ferrocement strengthened masonry infilled RC frame based on experimentally observed failure mechanisms". *Structures*, **58**, 105428. https://doi.org/10.1016/j.istruc.2023.105428

29 Kaya F, Tekeli H and Anil Ö (2018). "Experimental behavior of strengthening of masonry infilled reinforced concrete frames by adding rebar-reinforced stucco". *Structural Concrete*, **19**(6): 1792–1805. https://doi.org/10.1002/suco.201700210

30 Demirel IO, Yakut A, Binici B and Canbay E (2015). "An experimental investigation of infill behaviour in RC frames". *Proceeding of the 10th Pacific Conference on Earthquake Engineering*, Sydney, Australia, 1–8.

31 Altin S, Anil Ö, Kopraman Y and Belgin Ç (2010). "Strengthening masonry infill walls with reinforced plaster". *Institution of Civil Engineers: Structures and Buildings*, **163**(5): 331–342. https://doi.org/10.1680/stbu.2010.163.5.331

32 Zarnic R and Tomazevic M (1985). "Study of the behaviour of masonry infilled reinforced concrete frames subjected to seismic loading". *Proceeding of the 7th International Conference on Brick Masonry*, Melbourne, Australia, 1315–1326.

33 Alcocer SM and Flore L (2001). "Tests on connectors for seismic retrofitting of concrete and masonry structures in Mexico". *In International RILEM Symposium on Connections between Steel and Concrete*, (pp. 481–490). RILEM Publications SARL

34 American Society of Testing Materials (2011). "*Standard Test Method for Compressive Strength of Cylindrical Concrete Specimens"*. ASTM C39.

35 American Society of Testing Materials (2011). "*Standard Test Methods for Tension Testing of Metallic Materials"*. ASTM E8.

36 American Society of Testing Materials (2011). "*Standard Test Method for Compressive Strength of Masonry Prisms"*. ASTM C1314.

37 American Society of Civil Engineers (2013). "*Seismic Evaluation and Retrofit Rehabilitation of Existing Buildings"*. ASCE 41-13.

38 Paulay T and Priestley MJ (1992). *Seismic Design of Reinforced Concrete and Masonry Buildings*, New York, USA: John Wiley and Sons. https://doi.org/10.1002/9780470172841

39 Abrams DP, Angel R and Uzarski J (1996). "Out-of-plane strength of unreinforced masonry infill panels". *Earthquake Spectra*, **12**(4): 825-844. https://doi.org/10.1193/1.1585912

40 Dias-Oliveira J, Rodrigues H, Asteris PG and Varum H (2022). "On the seismic behavior of masonry infilled frame structures". *Buildings*, **12**(8): 1146. https://doi.org/10.3390/buildings12081146

41 The Japan Building Disaster Prevention Association (JBDPA) (2001). "*Guideline for Post-Earthquake Damage Evaluation and Rehabilitation".* (Revised in 2015) (in Japanese).

42 The Japan Building Disaster Prevention Association (JBDPA) (2001). "*Standard for Seismic Evaluation of Existing Reinforced Concrete Buildings".*

43 Sen D, Alwashali H, Tafheem Z, Islam MS, Maeda M and Seki M (2020). "Experimental investigation and capacity evaluation of Ferro-cement laminated masonry infilled RC frame". *Proceeding of the 17th World Conference on Earthquake Engineering*, Sendai, Japan.

ANNEXURE

Annexure A1: Specification of LVDTs

Name of LVDTs	Type	Specification
LVDT 1 LVDT 2	CDP-25 (CDP Displacement Transducer)	Capacity = 25 mm, Rated output (RO) = 12500×10^{-6} strain ± 0.1%, Sensitivity = 500×10^{-6} strain/mm, Calibration coefficient = 0.002 mm/(1x10^{-6}), Nonlinearity = 0.1% RO
LVDT 3 LVDT 4 LVDT 5 LVDT 6	CDP-100 (CDP Displacement Transducer)	Capacity = 100 mm, Rated output (RO) = 10000×10^{-6} strain ± 0.1%, Sensitivity = 100×10^{-6} strain/mm, Calibration coefficient = 0.01 mm/(1x10^{-6}), Nonlinearity = 0.1% RO

Annexure A2: Out-of-Plane Capacity Degradation of the Non-Strengthened Masonry Infill at Different In-Plane Story Drifts

Studying the out-of-plane behavior of masonry infill is an essential topic; however, it is out of the scope of this study. Therefore, in this section, an assessment of the out-of-plane capacity of the masonry infill of the specimen IM has been conducted to understand the degradation of out-of-plane capacity with the increase of in-plane story drift.

The out-of-plane capacity (q_u) has been evaluated as suggested by Abrams et al. [39]. The out-of-plane strength of the infill masonry at a certain in-plane story drift (Δ) can be estimated as per Equation A1-A3.

$$q_u = \frac{f_m}{\left(\frac{h}{t}\right)} R_1 R_2 \lambda \quad \text{(A1)}$$

$$R_1 = \left[1.08 - 0.015\left(\frac{h}{t}\right) - 0.00049\left(\frac{h}{t}\right)^2 + 0.000013\left(\frac{h}{t}\right)^3\right]^{\frac{\Delta}{2\Delta_{cracked}}} \quad \text{(A2)}$$

$$R_2 = 0.357 + (7.14\ x\ 10^{-8}) * EI \quad \text{(A3)}$$

where, f_m = masonry prism strength; h/t = height to thickness ratio of masonry infill; Δ = in-plane story drift; $\Delta_{cracked}$ = story drift at first cracking and EI = flexural rigidity of the smallest member of the surrounding frame.

The relative out-of-plane capacity, i.e., the ratio of out-of-plane capacity at a certain in-plane story drift to the out-of-plane capacity at the zero in-plane story drift, is plotted in Figure A1. It is evident that the non-strengthened masonry in the specimen IM is expected to lose almost 50% of its out-of-plane capacity at the story drift where the in-plane peak resistance of the masonry infilled RC frame was observed in the experimental program of this study.

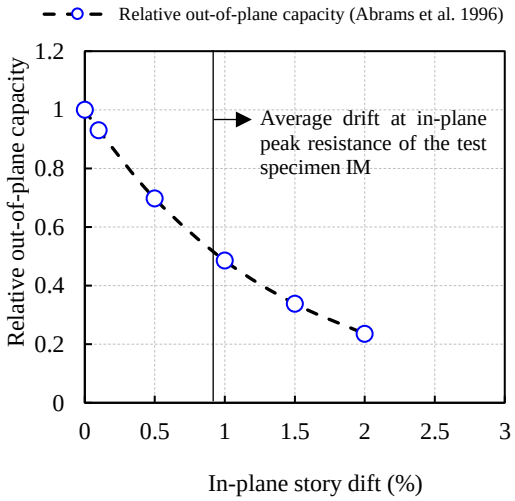

Figure A1: Out-of-plane capacity degradation of the non-strengthened masonry infill.